Tropospheric SF_6: Age of air from the Northern Hemisphere midlatitude surface

D. W. Waugh,[1] A. M. Crotwell,[2,3] E. J. Dlugokencky,[2] G. S. Dutton,[2,3] J. W. Elkins,[2] B. D. Hall,[3] E. J. Hintsa,[2,3] D. F. Hurst,[2,3] S. A. Montzka,[2] D. J. Mondeel,[2,3] F. L. Moore,[2,3] J. D. Nance,[2,3] E. A. Ray,[2,3] S. D. Steenrod,[4] S. E. Strahan,[4] and C. Sweeney[2,3]

Received 1 May 2013; revised 10 August 2013; accepted 16 September 2013; published 10 October 2013.

[1] Observations of SF_6 are used to quantify the mean time since air was in ("mean age" from) the Northern Hemisphere (NH) midlatitude surface layer. The mean age is a fundamental property of tropospheric transport that can be used in theoretical studies and used to evaluate transport in comprehensive models. Comparisons of simulated SF_6 and an idealized clock tracer confirm that the time lag between the SF_6 mixing ratio at a given location and the NH midlatitude surface provides an accurate estimate of the mean age. The ages calculated from surface SF_6 measurements show large meridional gradients in the tropics but weak gradients in the extratropics, with near-zero ages at the surface north of 30°N and ages around 1.4 years south of 30°S. Aircraft measurements show weak vertical age gradients in the lower and middle troposphere, with only slight increases of age with height in the NH and slight decreases with height in the Southern Hemisphere. There are large seasonal variations in the age at tropical stations (annual amplitudes around 0.5–1.0 year), with younger ages during northern winter, but only weak seasonal variations at higher latitudes. The seasonality and interannual variations in the tropics and Southern Hemisphere are related to changes in locations of tropical convection. There is qualitative agreement, in both spatial and temporal variations, between the simulated ages and observations. The model ages tend to be older than observed, with differences of ~0.2 year in the Northern Hemisphere upper troposphere and throughout the Southern Hemisphere troposphere.

Citation: Waugh, D. W., et al. (2013), Tropospheric SF_6: Age of air from the Northern Hemisphere midlatitude surface, *J. Geophys. Res. Atmos.*, *118*, 11,429–11,441, doi:10.1002/jgrd.50848.

1. Introduction

[2] Understanding and modeling tropospheric transport is important for a wide range of issues, including understanding and modeling air quality and the distribution of radiatively important gases and aerosols. Observations of trace gases provide one of the few ways to quantify transport within the atmosphere. A particularly useful tracer for evaluating large-scale transport is sulfur hexafluoride (SF_6). Atmospheric SF_6 has an extremely long lifetime (800–3200 years) [*Ravishankara et al.*, 1993; *Morris et al.*, 1995] and a large growth rate, and SF_6 observations can be used to calculate interhemispheric exchange times [e.g., *Geller et al.*, 1997; *Levin and Hesshaimer*, 1996] and to evaluate the transport in models [e.g., *Denning et al.*, 1999; *Peters et al.*, 2004; *Gloor et al.*, 2007; *Patra et al.*, 2009].

[3] A further use of SF_6 that appears not to have been explored is to estimate the mean time since air had contact with the surface layer in the midlatitudes of the Northern Hemisphere (NH) (mean age from the NH surface). As SF_6 has exhibited a near-linear growth rate over tropospheric transport time scales of 1–3 years and is emitted predominantly in NH middle latitudes (91% of emissions are between 20°N and 60°N [*EDGAR*, 2011]), the time lag between the SF_6 mixing ratio at a given location and that at the NH midlatitude surface provides an estimate of the mean age from the NH surface. This relationship will be confirmed in chemical transport model simulations presented below.

[4] As discussed above, several previous studies have used measurements of the SF_6 mixing ratio to calculate the interhemispheric exchange or to evaluate transport in models. Expressing the SF_6 observations as a mean age presents several advantages over analysis of the SF_6 mixing ratio. From a theoretical prospective, the mean age is a fundamental property of the transport that can be used in theoretical studies and

[1]Department of Earth and Planetary Sciences, Johns Hopkins University, Baltimore, Maryland, USA.
[2]Earth System Research Laboratory, NOAA, Boulder, Colorado, USA.
[3]Also at Cooperative Institute for Research in Environmental Sciences, University of Colorado Boulder, Boulder, Colorado, USA.
[4]Goddard Earth Sciences and Technology Center, Universities Space Research Association, Columbia, Maryland, USA.

Corresponding author: D. W. Waugh, Department of Earth and Planetary Sciences, Johns Hopkins University, 320 Olin Hall, 3400 N. Charles St., Baltimore, MD 21218, USA. (waugh@jhu.edu)

2169-897X/13/10.1002/jgrd.50848

Table 1. Surface Stations Used in This Study

ID	Station Name	Country	Network	Latitude	Longitude
SUM	Summit	Greenland	HATS[a]	72.6	−38.4
BRW	Barrow, Alaska	United States	HATS[a]	71.3	−156.6
MHD	Mace Head, Galway	Ireland	HATS	53.3	−9.9
THD	Trinidad Head, California	United States	HATS	41.0	−124.1
NWR	Niwot Ridge, Colorado	United States	HATS[a]	40.0	−105.5
KUM	Cape Kumukahi, Hawaii	United States	HATS	19.5	−154.8
MLO	Mauna Loa, Hawaii	United States	HATS[a]	19.5	−155.6
GMI	Mariana Islands	Guam	CCGG	13.3	144.7
RPB	Ragged Point	Barbados	CCGG	13.2	−59.4
CHR	Christmas Island	Republic of Kiribati	CCGG	1.7	−157.1
SEY	Mahe Island	Seychelles	CCGG	−4.7	55.5
ASC	Ascension Island	United Kingdom	CCGG	−8.0	−14.4
SMO	Tutuila	American Samoa	HATS[a]	−14.2	−170.6
CGO	Cape Grim, Tasmania	Australia	HATS	−40.7	144.7
TDF	Tierra Del Fuego, Ushuaia	Argentina	HATS	−54.8	−68.3
PSA	Palmer Station, Antarctica	United States	HATS	−64.9	−64.0
SPO	South Pole, Antarctica	United States	HATS[a]	−90.0	−24.8

[a]Stations with in situ measurements.

idealized models of tropospheric transport. As will be shown below, the mean age at the surface in southern high latitudes is similar to the interhemispheric exchange time calculated from surface measurements. However, the mean age can be calculated for locations throughout the troposphere and provides more information on transport times than the interhemispheric exchange time, which only quantifies the transport between hemispheres. Furthermore, knowledge of the mean age also has the potential to be useful for understanding the relative roles of transport and chemistry and for interpretation of observations of other tracers, e.g., knowledge of the mean age may help constrain the mean loss rate of nonconserved tracers.

[5] Recasting SF_6 as an age also presents some advantages over model-data comparisons of SF_6 mixing ratios. Previous comparisons of models with observed SF_6 require simulations for the particular years of the SF_6 measurements (which often vary between measurement data sets), and these simulations may not always be available (or possible) for all models. By converting to age, the values from different years can be averaged together to form a climatological data set that can then be more easily used to evaluate model simulations (assuming interannual variations, such as those related to El Niño–Southern Oscillation (ENSO), are small compared to model-data differences). This will be particularly advantageous for chemistry-climate models that calculate meteorological fields internally and do not use meteorology for a particular year. As the age is calculated relative to the modeled SF_6 concentrations, comparing age rather than absolute concentration may also reduce the sensitivity to the emissions used in the simulations (i.e., a bias in the mixing ratio in the source regions due to errors in emissions may not impact the age comparisons as much as comparisons of mixing ratios).

[6] Here we use surface and aircraft-based measurements of SF_6 to calculate, for the first time, the mean age from the NH midlatitude surface. We examine the spatial (latitude and vertical) and temporal (seasonal and interannual) variations in this age. We also examine a chemical transport model simulation of SF_6 to (i) show that the SF_6 age is a good estimate of the actual mean age from the NH midlatitude surface and (ii) illustrate the value of the observed SF_6 age for evaluating the large-scale transport in the model.

[7] The age considered here needs to be distinguished from SF_6-based estimates of the mean age of stratospheric air [*Harnisch et al*., 1996; *Patra et al*., 1997; *Ray et al*., 1999; *Engel et al*., 2006]. The same concepts are involved but we consider here transport from the NH midlatitude surface rather than the tropical tropopause (or tropical surface) as has been done in previous studies. Furthermore, given the shorter transport times within the troposphere, there is a much smaller impact of mesospheric losses or nonlinearity in the SF_6 growth on the derived tropospheric age. The age considered here should also be distinguished from the mean transport time from anywhere on the surface (e.g., the "tropospheric age of air" simulated by *Patra et al*. [2009]).

[8] The observations, model simulations, and details of the age calculations are described in the next section. In section 3, the age from surface and aircraft SF_6 observations is calculated, and the spatial and temporal variations are examined. In section 4, model simulations are examined and compared with the observed ages. Concluding remarks are in section 5.

2. Methods

2.1. Observations

[9] The SF_6 measurements examined here were made by several instruments operated by groups at the NOAA Earth System Research Laboratory Global Monitoring Division (ESRL GMD) and include ground-based, ship-borne, and aircraft measurements.

[10] The NOAA Halocarbons and other Atmospheric Trace Species (HATS) group measure SF_6 quasi-continuously from in situ instruments and from discrete samples collected in flasks, at 12 stations ranging in latitude from the Arctic to the South Pole [*Geller et al*., 1997; *Hall et al*., 2011] (see Table 1 and Figure 1). Flask measurements started in 1995 with eight stations and continue today, sampling at 12 remote locations. A four-channel gas Chromatograph for Atmospheric Trace Species (CATS) was developed in 1998 and is currently deployed at six field sites and makes hourly measurements. The HATS data used are monthly mean combined flask and in situ SF_6 measurements from these 12 stations.

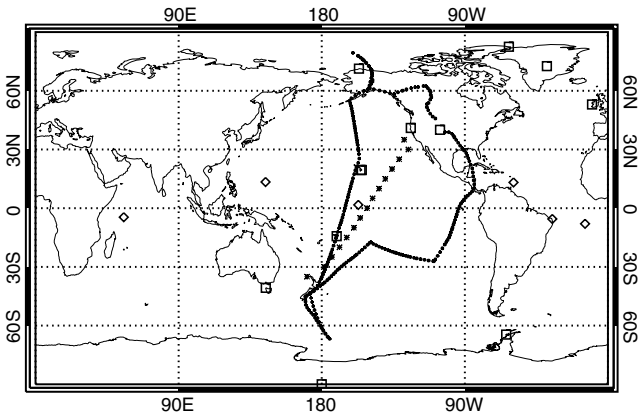

Figure 1. Map of locations of ground stations (HATS: square; CCGG: diamond), ship cruises (asterisk), and aircraft flights (cross) of SF_6 observations.

[11] The HATS network does not sample within the tropics; however, the NOAA Carbon Cycle Greenhouse Gases (CCGG) group has made regular SF_6 measurements from discrete air samples collected at several tropical sites and from ships crossing the equatorial Pacific [*Peters et al*., 2004]. We examine CCGG measurements of SF_6 from the tropical sites listed in Table 1 (which have long data records covering 1995 or 1997 to 2012), as well as measurements in the eastern Pacific Ocean from commercial ships (measurements are made approximately every 5° between 35°S and 35°N, from 1995 to 2012). Monthly mean values are used for the terrestrial sampling sites, but (given limited sampling for any given latitude and month) we use individual measurements for the ship data.

[12] In addition to the above surface measurements, we consider aircraft measurements made as part of the HIAPER Pole-to-Pole Observations (HIPPO) project [*Wofsy*, 2011; *Wofsy et al*., 2012]. HIPPO consists of five aircraft campaigns that measured atmospheric composition approximately pole-to-pole (~80°N to ~70°S), from the surface to the tropopause, during different seasons over a 3 year period (January 2009 to September 2011). Figure 1 shows the flight paths for the first campaign (similar flights were made for all campaigns). Several instruments made SF_6 measurements on these flights. In situ measurements were made using the PAN and Other Trace Hydrohalocarbon Experiment (PANTHER) [*Elkins et al*. 2002; *Wofsy*, 2011] and the Unmanned Aircraft Systems Chromatograph for Atmospheric Trace Species (UCATS) [*Moore et al*. 2003; *Fahey et al*. 2006; *Wofsy*, 2011] instruments, and measurements from flasks collected with an onboard NOAA whole air sampler (NWAS) were analyzed by the CCGG. (Additional whole air samples were also taken by the University of Miami but are not included here.)

[13] All the above measurements are reported relative to the same NOAA 2006 calibration scale. Scale transfer uncertainties are 0.03–0.05 parts per trillion (ppt) prior to 2003, and approximately 0.02 ppt from 2003 to present. The repeatability of the measurements varies between instruments (and over time) but is around 0.03–0.05 ppt (1σ). The SF_6 mixing ratio increases from around 2 ppt to 7 ppt between 1990 and 2010, with growth rate of SF_6 varying between 0.20 and 0.30 ppt/yr (~4–7%/yr) (see Figure 2b). So the uncertainty in the SF_6-derived age is around 0.1–0.2 year.

2.2. Model Simulations

[14] We examine a simulation of SF_6 performed using the Global Modeling Initiative three-dimensional chemical transport model [*Strahan et al*., 2007] driven by meteorological fields from the Modern-Era Retrospective Analysis for Research and Applications (MERRA) reanalyses [*Rienecker et al*., 2011] (referred to here as the "GMI-MERRA" model). The SF_6 simulation was performed with horizontal resolutions of 2° latitude by 2.5° longitude and 72 levels extending from the surface up to 0.01 hPa. The SF_6 simulation was spun up for 8 years and then integrated forward from 1990 using MERRA fields. The SF_6 emissions are based on the Emission Database for Global Atmospheric Research 2000 using the temporal scaling factors in Table 2 of *Levin et al*. [2010] (assuming a constant scaling after 2008). The simulations also include stratospheric and mesospheric loss, which is assumed to be similar to that of CFC-115. This results in a global lifetime of

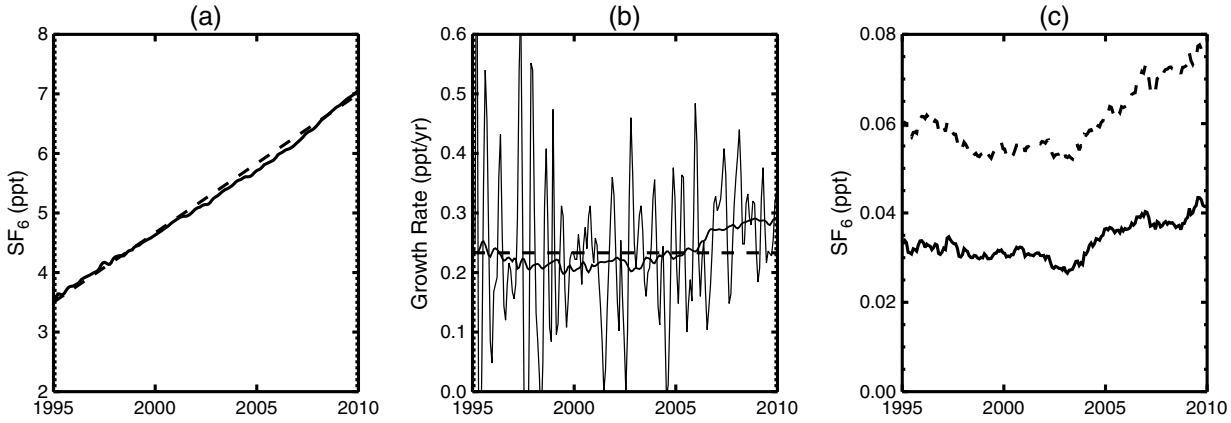

Figure 2. SF_6 reference time series. (a) Time series of average SF_6 from surface measurements at the NWR, THD, and MHD stations (see Table 1). Dashed line is the linear fit to the time series. (b) Growth rate of time series in Figure 2a; dashed line is average growth rate and thick curve is the time-averaged growth rate. (c) Difference in time-averaged (23 month smoothed) simulated surface SF_6 between zonal-mean and station averages (solid) and between land-only and station averages (dashed), see text for details.

515 years, which is smaller than the estimated lifetime of 800 to 3200 years [*Ravishankara et al*., 1993; *Morris et al*., 1995].

[15] We also examine a GMI-MERRA simulation of an idealized "NH-clock" tracer. This tracer is initially zero throughout the atmosphere and is held at zero in the surface layer between 30° and 50°N with a constant aging of 1 year per year in the rest of the surface layer and throughout the atmosphere. When the tracer reaches a steady value, it is equivalent to the mean age from the NH midlatitude (30–50°N) surface. The tracer integration was performed from 2004 to 2010, and we analyze the last year of the integration. (Similar clock tracers with different reference regions, e.g., tropical tropopause, are used to calculate the stratospheric mean age [e.g., *Neu and Plumb*, 1999] and are also used in ocean studies (where the resulting age/time is referred to as the "ideal age") [e.g., *England*, 1995].) Comparison of the NH-clock tracer with the SF_6 simulation shows how well the SF_6 age approximates the mean time since the air was in contact with the NH midlatitude surface layer.

2.3. Age Calculations

[16] We calculate the "SF_6 age" from both the observed and modeled SF_6 fields. The age at a particular location, $a(x)$, is defined as the time since the SF_6 mixing ratio in the "source region" equaled the mixing ratio at that location, i.e.,

$$C(x,t) = C_0(t - a(x,t)), \tag{1}$$

where C is the SF_6 mixing ratio at location x and C_0 the mixing ratio in the source region. If the tracer has a constant, linear growth rate (dC/dt), the age can be reexpressed as

$$a(x) = \frac{(C(x) - C_0)}{dC_0/dt}. \tag{2}$$

[17] Although Equation (2) is a reasonable approximation for the age, we use Equation (1) in our calculations to take account of changes in dC_0/dt over time.

[18] There are several factors that cause uncertainties in the SF_6 age calculation. One is the definition of the reference source time series C_0. Ideally, the mixing ratio of the age tracer is uniform within a particular source region, and C_0 would be the time series of this uniform mixing ratio. However, the emissions of SF_6 are not uniform, and the average mixing ratio over a specified region has to be used instead. A further complication when applying this to observations is that long-term measurements of SF_6 are available from only a few NH midlatitude sites, and it is not possible to calculate an observationally based area average reference time series.

[19] In the age calculations from SF_6 observations, we use the average mixing ratio from the three HATS northern midlatitude stations: Mace Head (MHD), Trinidad Head (THD), and Niwot Ridge (NWR) stations (Table 1 and see Figure 2a). MHD and THD are coastal stations (western Ireland and USA, respectively), and NWR is a high-altitude station within the continental USA

[20] For the age calculations using the simulated SF_6, it is possible to calculate many different reference series, as we have SF_6 values at all grid locations. Figure 2c shows the difference in simulated SF_6 mixing ratio between three reference series: the average of surface values over the location of the above three stations ("station" reference), the average surface value over 30–50°N (zonal mean), and the average over land within 30–50°N (land only). The land-only SF_6 is larger than the zonal-mean average, which is in turn larger than the average over the stations. These differences occur because the source regions of SF_6 are over land (so the land-only average is larger than the zonal mean) and the stations are either coastal or high-elevation locations that are not near the major source regions. The differences between the references change with time (e.g., are larger in 2005–2010 than in 1995–2000), because of changes in the spatial distribution of emissions over time.

[21] For a given observed SF_6 mixing ratio, the use of a reference time series with higher values results in an older age (i.e., there is a larger elapsed time since the observed value occurred in the source region). For example, the use of a reference time series with values larger by 0.04 ppt will, assuming an approximate SF_6 growth rate of 0.3 ppt/yr, increase the calculated age by around 0.13 year. The approximate difference between the references time series shown in Figure 2c is around 0.04 ppt around 2010 and the growth rate is around 0.3 ppt/yr (Figure 2b), so we expect the use of the different reference time series to causes differences in calculated SF_6 age by around 0.15 year.

[22] When comparing the age from the SF_6 simulation with the age from observations, we use the station reference times to calculate the age (so there is consistency between the age calculations), whereas for comparisons with the idealized NH-clock tracer (which has a uniform source covering 30–50°N), we use either the zonal-mean or the land-only reference time series.

[23] Another cause of uncertainty in the age calculation is the nonlinear growth of the mixing ratio in the source region. Figure 2a shows that the increase in SF_6 mixing ratio is close to linear. However, there are seasonal as well as longer time scale variations in the growth (see Figure 2b). These variations can be related to changes in the SF_6 emissions. For example, there was decrease in annual-mean emissions from around 1995 to around 2000, with an increase in subsequent years [e.g., *Levin et al*., 2010], and there is corresponding change in the annual-mean SF_6 growth rate (Figure 2b). The impact of these nonlinear variations is discussed below and in Appendix A.

2.4. Interhemispheric Exchange Time

[24] As several previous studies have calculated an interhemispheric exchange time τ_{ex} from surface measurements of SF_6, we briefly discuss the relationship between the SF_6 age and τ_{ex}. The interhemispheric exchange time τ_{ex} can be written as [*Patra et al*., 2009]

$$\tau_{ex} = \Delta C \left(\frac{E_n}{E_s} + 1\right) \Big/ \left(\frac{E_n}{E_s}\frac{dC_s}{dt} - \frac{dC_n}{dt}\right), \tag{3}$$

where C is the hemispheric mean tracer mixing ratio ("n" and "s" refer to averages over the Northern and Southern Hemispheres, respectively), E is the hemispheric tracer emission, and $\Delta C = C_n - C_s$. As the NH sources are 97% of total SF_6 emissions and atmospheric SF_6 is very long-lived, $E_n >> E_s$, $dC_s/dt \approx dC_n/dt \approx$ constant, and

$$\tau_{ex} \approx \frac{\Delta C}{dC/dt}. \tag{4}$$

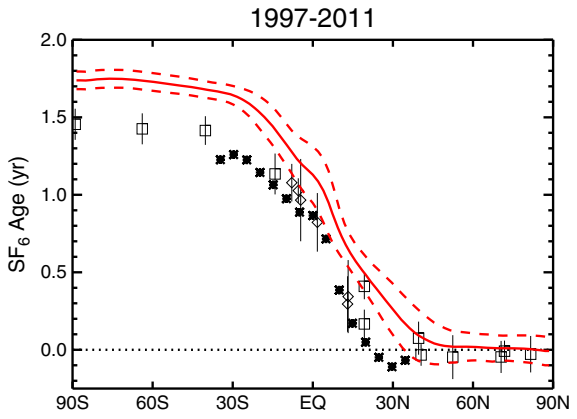

Figure 3. Latitudinal variation of climatological-mean surface SF_6 age calculated from measurements at ground stations (HATS: square; CCGG: diamond) or ship cruises (asterisk). Vertical bars show ±1 standard deviation. Red curves show surface SF_6 age at 180°W from the GMI-MERRA model (solid curve is mean and dashed curves are ±1 standard deviation).

[25] In the above expressions, C is the mean mixing ratio averaged over one hemisphere (or equivalently the hemispheric mass of the tracer). However, measurements of SF_6 are generally not available throughout the troposphere, and previous studies have generally used measurements of surface mixing ratios as estimates of C_n and C_s [e.g., *Geller et al.*, 1997; *Levin and Hesshaimer*, 1996; *Patra et al.*, 2009]. There are larger interhemispheric gradients at the surface than at higher altitudes (see below), and the use of surface mixing ratios for C results in an overestimate of τ_{ex} [*Denning et al.*, 1999]. However, to enable comparisons with previous observational estimates, we consider surface-based calculations of τ_{ex}.

[26] If we replace C in 4 with mean surface mixing ratios and, in addition, assume (i) the NH average mixing ratio is similar to that of the source region used for SF_6 age calculations here, i.e., $C_0 \sim C_n$, and (ii) C in southern middle-high latitudes is similar to the Southern Hemisphere (SH) average, then 4 reduces to 2. This implies that the SF_6 age at SH high latitudes will be similar to calculations of τ_{ex} based on surface measurements. An exact correspondence between the age and τ_{ex} is not expected as both 2 and 4 are approximate expressions.

3. Observations of SF_6

[27] We first examine the age calculated from surface SF_6 measurements. The symbols in Figure 3 show the 1997–2011 climatological mean ages for the stations shown in Figure 1 (and listed in Table 1). The observations from different stations and networks generally agree well and show a consistent picture. (There is a significant difference in age between the two Hawaiian stations (19.5°N), which is due to differences in altitude of the stations, with higher ages at the higher MLO station (elevation around 3400 m).) The observations show very weak meridional age gradients in the extratropics of both hemispheres but a large gradient within the tropics. In northern middle and high latitudes, the age is very close to zero, and there is a large increase in the age between 30°N and 30°S, with age ~1 year at the equator and ~1.4 years in the southern extratropics.

[28] There is some sensitivity of the absolute value of the age to the reference time series used in the age calculations. The slightly negative mean values for the age at most of the NH middle and high latitude stations shown in Figure 3 are due to the inclusion of the higher altitude NWR data in the reference time series. If NWR were not included, the reference SF_6 would be higher and the age at other stations would be closer to zero. (Note that we have included NWR in the calculation of the reference time series as it represents the longest data record in the northern midlatitudes.)

[29] The latitudinal variations shown in Figure 3 are consistent with previous studies that have shown near-uniform high surface SF_6 mixing ratios in NH middle and high latitudes, and significantly lower values in SH middle and high latitudes [e.g., *Denning et al.*, 1999; *Peters et al.*, 2004; *Gloor et al.*, 2007]. Furthermore, the ages of 1.3–1.4 years in SH middle and high latitudes are also consistent with previous estimates of τ_{ex} = 1.3–1.5 years from surface SF_6 observations [e.g., *Geller et al.*, 1997; *Levin and Hesshaimer*, 1996; *Patra et al.*, 2009].

[30] Figure 3 shows the climatological mean SF_6 age, but there are also seasonal and interannual variations. These can be seen in Figure 4, which shows the evolution of the SF_6 age at several stations. We focus here on stations south of 20°N, as the age at higher latitudes is close to zero and sensitive to the reference time series used. The seasonal variations in the age are largest within the tropics: The peak-to-peak amplitude in the climatological mean seasonal cycle varies between 0.4 and 0.8 year for tropical stations, whereas the peak-to-peak amplitude is around 0.15 year or less for stations outside the tropics (see Figure 5). While the seasonal variations are largest in the tropics, the seasonal amplitude is not simply a function of distance from the equator. The largest seasonal amplitude occurs at Mahe Island, Seychelles (SEY; 5°S), and the amplitude here is roughly twice that at the Christmas Island equatorial station (CHR; 1.7°N). Also, there is a difference in the two stations near 13°N (GMI and RPB). The large seasonal variations of SF_6 at these stations were described by *Gloor et al.* [2007] and related to the seasonal movement of the Intertropical Convergence Zone (ITCZ; see Figure 8 below). At all tropical stations, the seasonal minimum age occurs during NH winter, when the ITCZ is south of the stations and there are northerly surface winds (and more rapid transport from NH midlatitudes). The seasonal variation at SEY is larger because the seasonal variation in the latitude of the ITCZ is larger than at the longitudes of the other stations. See further discussion below in the modeling section.

[31] At all stations, there are interannual variations in age (Figure 4). Within the tropics, the amplitude of these variations is smaller than the seasonal variations (Figure 5), but at southern middle and high latitudes, the multiyear and seasonal variations are comparable. There are some similarities among the multiyear variations at different stations, with most stations showing local minima around 2000 and 2008. Previous studies have noted a connection between observed variations of trace species at Samoa and the El Niño–Oscillation (ENSO) [e.g., *Elkins et al.*, 1993; *Prinn et al.*, 1992], and the modeling study of *Lintner et al.* [2004] showed faster interhemispheric transport during La Niña winters (December–February). As 2000 and 2008 correspond to periods of the negative ENSO phase (La Niña), the minima in the time-averaged age around these periods are consistent with a possible connection between age and ENSO. This is explored further below using the model simulation.

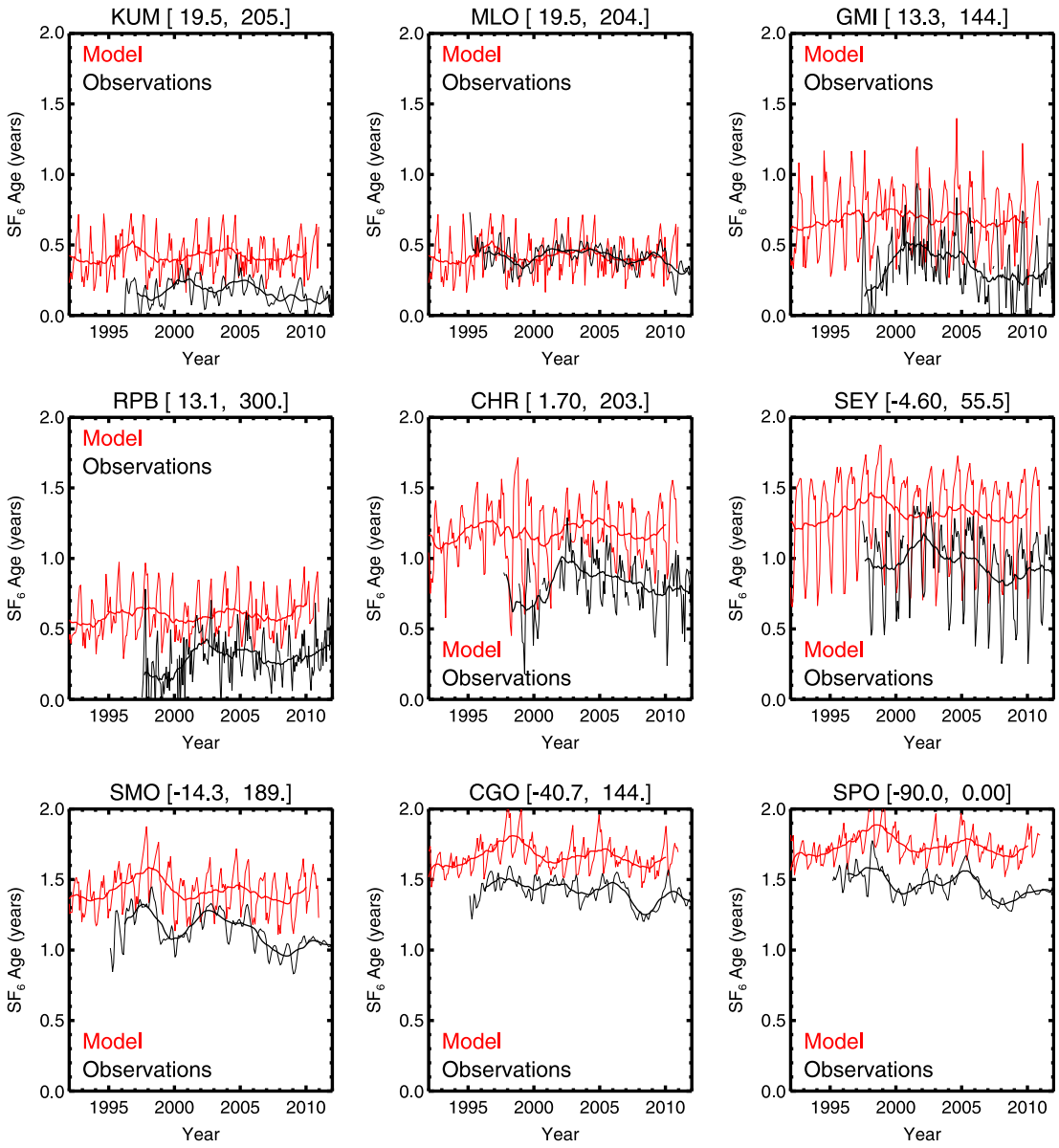

Figure 4. Temporal variations of SF_6 age at several surface locations for observations (black) and model (red). Plots titles list ID, latitude, and longitude of the locations. Thick curves show 23 month running mean values. Model values are for lowest level in the model (and values are same for KUM and MLO).

[32] A complication with the interpretation of the temporal variations in the SF_6 age is the possible impact of nonlinear variations in the reference SF_6 time series. The temporal variation in SF_6 within the source region is not exactly linear (Figure 2), and, as discussed in *Waugh et al*. [2003], nonlinearities in the tracer history can cause temporal changes in the tracer time lag (age) even for steady flow. As discussed in Appendix A, the observed seasonal and interannual variations in the tropics are unlikely to be caused by nonlinearities in SF_6 growth, but some of the multiyear variations in SF_6 age at middle and high southern latitudes may be artifacts of these nonlinearities.

[33] We now examine vertical variations in age using HIPPO data. Figure 6 shows vertical profiles of the age for HIPPO-1 (January 2009) data in different latitude bins. The in situ measurements are averaged within 2 km bins, but because there are fewer whole air sample measurements, these are shown as individual points. There is good agreement among the three aircraft instruments, with all showing the same vertical and latitudinal variation in SF_6 (age). There is also good agreement with the surface station measurements (not shown).

[34] There are very weak vertical gradients in age below 8 km except in the northern subtropics, where there is a moderate increase in age with height (~0.5 year over the lowest 4 km), consistent with the differences in age between the two Hawaiian surface stations (see above). Although the vertical gradients are weak, there is a slight change with latitude, with positive age gradients (older air aloft) in the NH (especially around 20–30°) and negative gradients south of 20°S. This

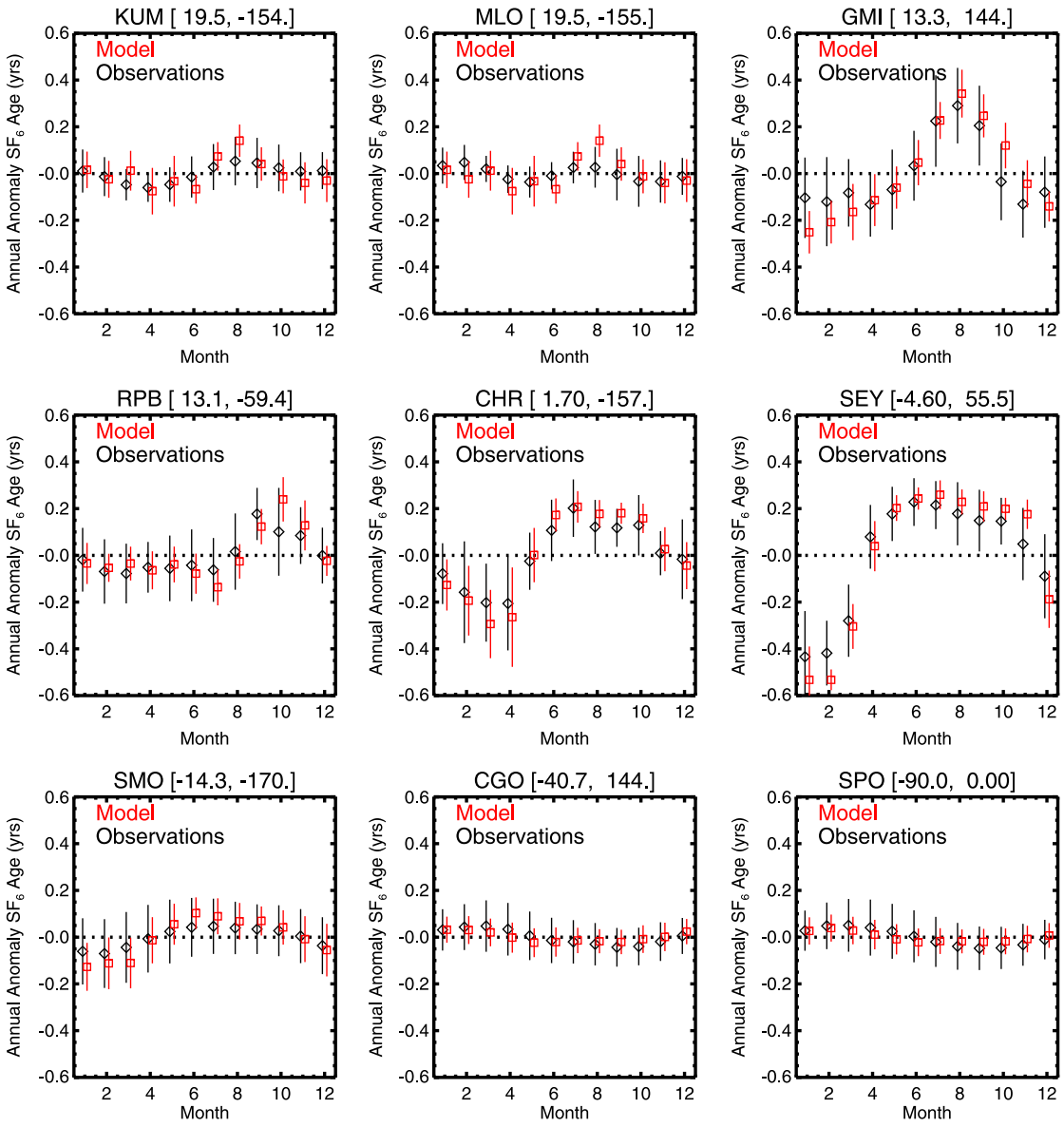

Figure 5. Climatological seasonal cycle of SF_6 age at the same surface locations as shown in Figure 4 for observations (black) and model (red). Symbols show the deviation of the climatological mean for each month from the climatological annual mean, while vertical bars show ±1 interannual standard deviation. Data and model output from 1998 to 2010 used for all calculations.

means that the meridional age gradients in the lower and middle troposphere are similar to that observed at the surface but weaken with height.

[35] Larger vertical gradients are found above 8 km in middle and high NH latitudes and high SH latitudes. These gradients are associated with the transition from upper tropospheric to (older) lower stratospheric air. The increase to large values occurs at lower altitudes for higher latitudes, consistent with a lower tropopause (see horizontal lines in Figure 6) and older stratospheric air at high latitudes.

[36] The spatial variations shown in Figure 6 are robust among instruments and measurement campaigns. Similar weak vertical gradients are found for SF_6 measurements from the three different instruments and for all HIPPO campaigns. Weak vertical gradients in SF_6, which change sign between hemispheres, are also observed in the long-term aircraft measurements made by the NOAA CCGG group (in Alaska, Harvard Forest, Hawaii, and Rarotonga) [see, for example, *Peters et al.*, 2004, Figure 5; *Gloor et al.*, 2007, Figure 7]. Furthermore, upper tropospheric (~10 km) SF_6 measurements on commercial aircraft flying between Germany and South Africa show a meridional gradient that is around half of that at the surface [*Gloor et al.*, 2007], consistent with the HIPPO data.

[37] The variations in age described above are consistent with our understanding of the large-scale tropospheric transport. There is rapid mixing between surface and middle troposphere in the northern extratropics (weak horizontal and vertical age gradients in the extratropical lower and middle troposphere), slower transport between hemispheres (larger tropical and subtropical gradients), and more rapid transport into the southern extratropics via the upper troposphere than

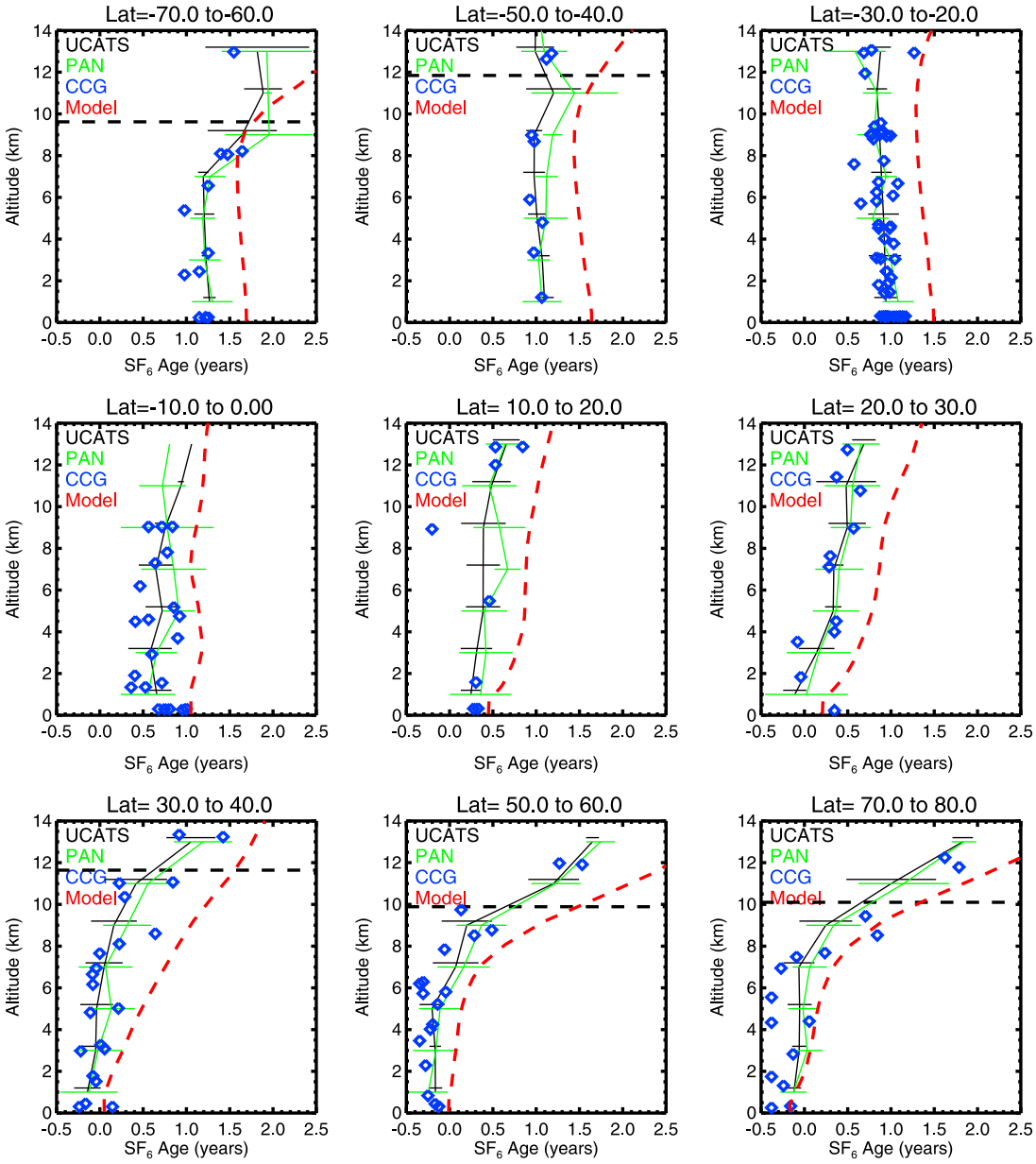

Figure 6. Vertical profiles of SF_6 age from HIPPO-1 (January 2009): UCATS (black), PANTHER (green), and CCGG whole air samples (blue symbols). Red curves are age at 180°W from the model. Horizontal dashed lines show the tropopause (for tropical and subtropical latitudes, the tropopause is above 14 km).

near the surface (younger age aloft at southern midlatitudes). There is also significant transport of stratospheric air into the extratropical upper troposphere (older air in the upper troposphere).

4. Simulations of Tropospheric Age

[38] We now consider the GMI-MERRA simulation of SF_6. We first test how well the age inferred from simulated SF_6 matches the simulation of the clock tracer and then compare the simulated SF_6 age with observations.

4.1. Comparisons With Clock Tracer

[39] Figure 7a shows pressure-altitude variations of the simulated annual and zonal mean SF_6 in 2009. The highest values of SF_6 occur at the Northern Hemisphere middle and high latitude surface, and there are decreasing surface values with more southerly latitudes. The vertical gradients change with latitude, with negative vertical gradients in the NH, very weak vertical gradients in the tropics, and positive vertical gradients in southern midlatitudes. These spatial variations of SF_6 are similar to those in previous SF_6 simulations [e.g., *Denning et al.* 1999, *Patra et al.*, 2009].

[40] The distribution of the SF_6 age (solid contours) and clock tracer (dashed contours) is shown in Figure 7b. There is good agreement between the clock and SF_6 ages, with both showing similar spatial variations to the SF_6 concentration, except with reversed sign of the gradients. In both calculations, there is a large increase in the surface age between 30°N and 30°S, with weaker meridional gradients in the

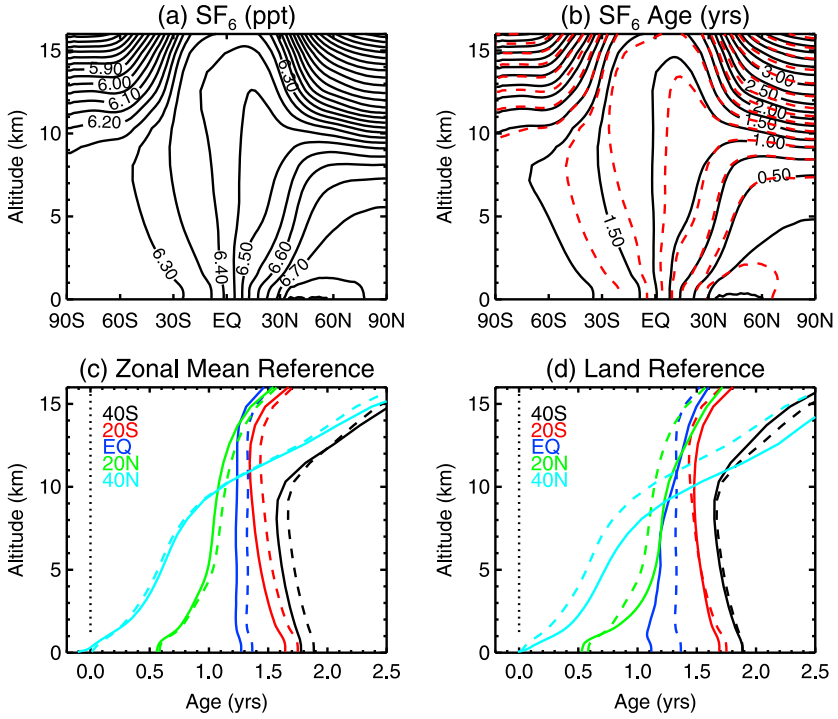

Figure 7. Simulations of SF_6 (solid curves) and clock tracers (dashed). (a) Annual-mean zonal-mean SF_6 concentration (0.05 ppt contour interval). (b) Annual-mean zonal-mean SF_6 age (solid) and clock age (dashed) (0.25 year contour interval). The zonal-mean reference time series is used for the SF_6 age calculation. (c, d) Vertical profiles of age SF_6 age (solid) and clock age (dashed) at 40°N (cyan), 20°N (green), 0°S (blue), 20°S (red), and 40°S (black), for SF_6 age relative to (c) zonal-mean and (b) land-only reference regions.

middle and upper troposphere. Also, in both age fields, there are positive vertical gradients in the NH and negative vertical gradients (upper troposphere younger than surface) in the SH, with strongest vertical gradients in the northern subtropics. The mean age shown in Figure 7b also agrees well with the mean age simulation shown in Figure 5 of *Holzer and Boer* [2001], with similar vertical and meridional gradients. The age in the *Holzer and Boer* [2001] simulation tends, however, to be around a year older. This could be due to differences in the models or to a more polar source region in their simulation (north of 45°N rather than 30–50°N).

[41] While there is good agreement between the clock and SF_6 ages in Figure 7b, the SF_6 age is systematically younger than the clock in the SH. This is shown more clearly in Figure 7c, which compares vertical profiles of the zonal-mean age at several latitudes. As discussed in section 2.3, a complication in the SF_6 age calculation is the reference time series used. In Figures 7b and 7c, we have used the zonal-mean SF_6 averaged between 30 and 50°N, but if the land-only average is used, the calculated SF_6 age is older by around 0.1–0.15 year (consistent with discussions in section 2.3) and the SF_6 age is now older than the clock in the NH but agrees well in the SH (see Figure 7d).

[42] The SF_6 simulation includes stratospheric and mesospheric loss that reduces the SF_6 mixing ratio and increases the SF_6 age. The comparison with the clock tracer indicates this has a negligible impact within the troposphere but does have an impact in the stratosphere where the SF_6 age (for both reference time series) is systematically older than the clock tracer (not shown).

[43] The overall good agreement between the tropospheric age from the simulated SF_6 and the clock tracer indicates that the age from SF_6 is a good estimate of the mean age of air from the NH midlatitude surface. There is a small uncertainty in the age of around 0.10–0.15 year due to spatial variations in the surface SF_6 in NH midlatitudes.

4.2. Comparisons With Observations

[44] We now use the SF_6 observations to evaluate the transport time scales within GMI-MERRA. For these comparisons, we use a reference time series formed by averaging the simulated SF_6 mixing ratio at the location of the NH midlatitude stations. As discussed in section 2.3, this average is less than the NH midlatitude average used for the above comparison with the clock simulation (as the stations are mostly at locations away from main emission regions), which results in lower values of the SF_6 age.

[45] Overall, there is good qualitative agreement in the spatial variations of the SF_6 age between the model and observations. As in the observations, there are strong north-south gradients in the modeled age within the tropics but weak meridional gradients in middle and high latitudes (see red curves in Figure 4). (As most of the observations are from the Pacific Ocean or other oceans, the model ages shown are those at 180°W.) Also, the model age has weak vertical gradients, with positive vertical gradients in the NH and negative gradients in the SH (Figure 6). There are however some quantitative differences, with the model ages older than observed, both in the northern middle upper troposphere and throughout the Southern Hemisphere. In the Northern Hemisphere,

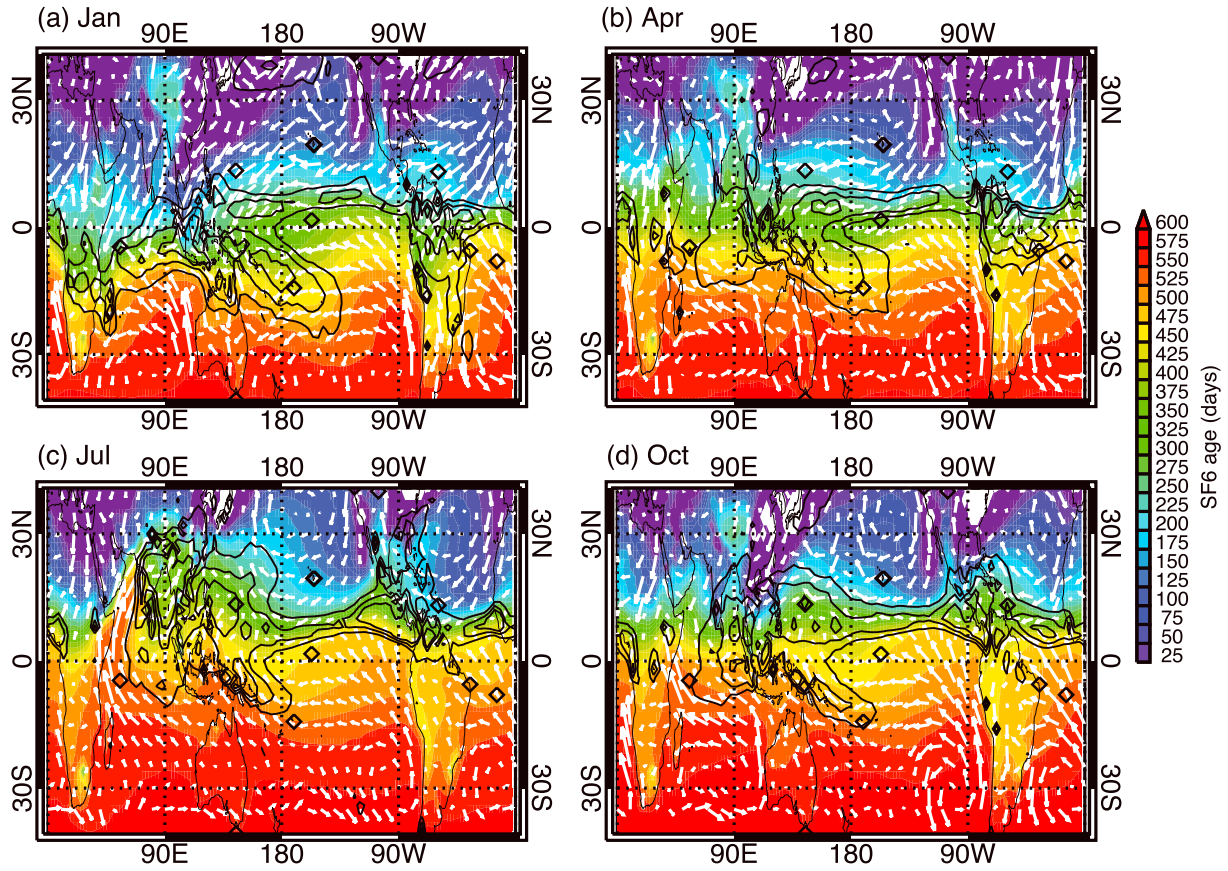

Figure 8. Maps of climatological-mean simulated surface SF_6 age (colors), reanalysis surface precipitation flux (black contours; contours for 6, 9, and 12 × 10^{-5} kg/m^2/s), and surface winds (arrows), for January, April, July, and October.

the vertical gradients in the middle troposphere are generally larger than observed, and the upper tropospheric age is older than observed. In the southern extratropics, the SF_6 age in the model is around 0.2–0.3 year older than observed, for all altitudes. Whether this bias is because the simulated transport within the troposphere is too slow or because there is too much transport of (old) stratospheric air into the troposphere (or a combination of both) is not known.

[46] While there are differences in the absolute magnitude, there is very good agreement between observed and simulated seasonal variations of the SF_6 age, both in terms of timing of seasonal maximum and annual amplitude (see Figure 5). This suggests that the GMI-MERRA is correctly simulating seasonal variations in transport through the tropics.

[47] As discussed in section 3, seasonal variations in SF_6 have been linked to the movement of the ITCZ [*Gloor et al.*, 2007]. We explore this further using the GMI-MERRA simulation. Figure 8 shows maps of climatological mean simulated SF_6 age together with precipitation and surface winds from MERRA, for four different months. In general, there are large meridional age gradients at latitudes with large precipitation and surface convergence, with young ages to the north and older ages to the south of the region of precipitation. (There is good agreement between precipitation from MERRA and the Global Precipitation Climatology Project (GPCP) [*Adler et al.*, 2003], and the same correspondence between age gradients and precipitation is found using the GPCP data.) The latitude and strength of the age gradients varies between regions and with season. The largest seasonal variation in latitude of the precipitation and in the direction of surface winds occurs over the Indian Ocean. Consistent with this, there is a large seasonal cycle in SF_6 age at SEY: For around half of the year, SEY is north of the ITCZ, while for the remainder, it is south of the ITCZ. There is only weak seasonality in location of convection over the eastern Pacific, but there is seasonality in the strength, with corresponding variation in age gradients (i.e., weaker convection and weaker age gradients during January). More analysis is needed to determine the exact processes involved, but these maps suggest that seasonal variations in the surface convergence and convection explain most of the seasonality in surface age.

[48] There is less agreement between the observed and simulated multiyear variations in age. For some stations, there is good agreement (e.g., MLO and SMO) whereas for others, there are large differences (e.g., late 1990s in tropical stations; see Figure 4). The cause for these differences is unknown. Errors in the model transport are the likely cause. However, comparisons of MERRA and GPCP precipitation indicate that the MERRA reanalyses are capturing the correct interannual variations in the ITCZ. It is possible that some of the differences could also be due to changes in the measurements. In particular, the calibration strategy for the CCGG SF_6 measurements changed in the early 2000s and the uncertainty in the data prior to 2005 is larger than that for more

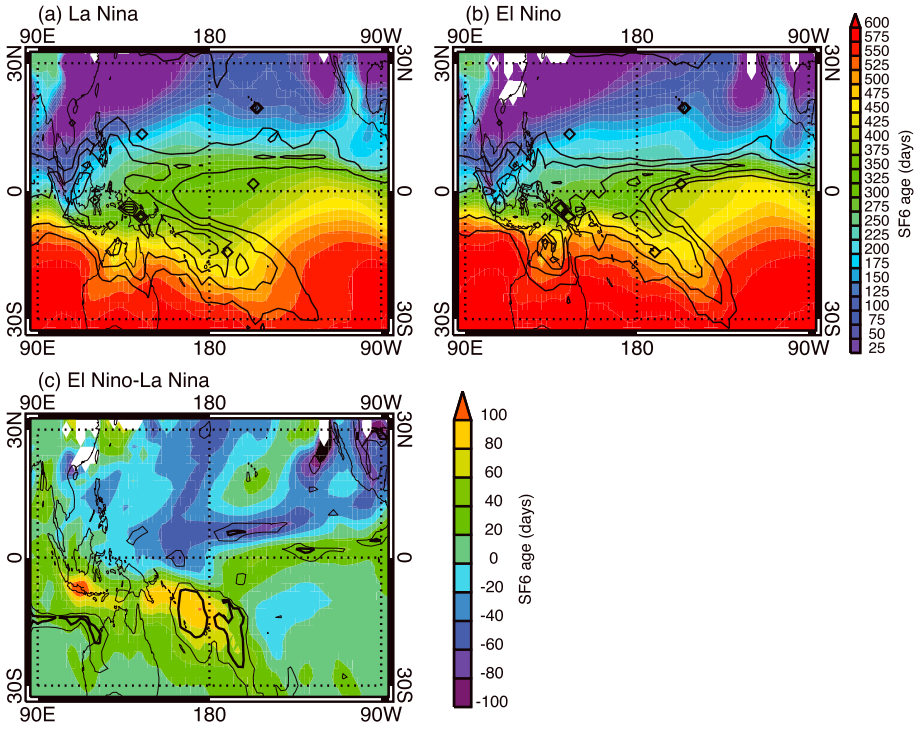

Figure 9. Maps of simulated surface SF_6 age (colors) and reanalysis precipitation (black contours) for average over (a) January 2000, 2008, and 2009, and (b) January 2003, 2007, and 2010. Same contouring as in Figure 8. (c) Difference between Figures 9a and 9b, with thin (thick) contour showing regions where difference is significant at the 5% (1%) level.

recent data. This could potentially explain the lower age values before and around 2000 in the CCGG data (GMI to SEY stations).

[49] As discussed above, interannual variations in the abundance of trace species in the tropics and subtropics have been linked to ENSO. To explore this, we compare composite fields for La Niña and El Niño years. Figure 9 shows maps (over the tropical Pacific) of GMI-MERRA SF_6 age and GPCP precipitation for January average over (a) three La Niña years (2000, 2008, and 2009) and (b) three El Niño years (2003, 2007, and 2010). As expected, there is more precipitation over the tropical eastern Pacific during El Niño years (i.e., convection and ITCZ extend farther to the east). There is a corresponding difference in the age over the eastern Pacific, with stronger meridional gradients, younger ages in the northern tropics, and older ages in the southern tropics during El Niño (see Figure 9c). Given that there are only three El Niño and three La Niña winters, most of the differences in Figure 9c are not statistically significant (the contours show the regions where the differences are statistically significant at the 1% or 5% level), and more analysis is required to better quantify the impact of ENSO on the age.

5. Concluding Remarks

[50] Using surface and aircraft SF_6 measurements, we have estimated the mean time (age) since air was at the NH midlatitude surface. The observations show large surface meridional gradients in the tropics but weak gradients in middle and high latitudes, with ages ~0 year north of 30°N and ~1.4 years south of 30°S. There are very weak vertical gradients in the lower and middle troposphere, with only a small increase of age with height in the NH and slight decreases with height in the SH. As a result, the large-scale meridional gradients in the lower and middle troposphere are similar to that at the surface. Significant vertical gradients are found only in the upper troposphere/lower stratosphere.

[51] The SF_6 observations show some temporal variations in age. There are large seasonal variations (annual amplitudes around 0.5–1.0 year) at tropical stations, with younger ages during northern winter. There are much weaker seasonal variations in the subtropics and higher latitudes, but there are coherent multiyear variations in the age observed at SH surface stations with a tendency for younger ages during La Niña years. Both the seasonal and ENSO variations in age appear linked to movement of the ITCZ, with younger ages (more rapid transport from NH midlatitudes) when the ITCZ is south of the station.

[52] The observations of the tropospheric age presented here are useful for evaluating the transport in models. This has been illustrated by comparison with simulations by the Global Modeling Initiative model driven by MERRA meteorological fields. There is qualitative agreement between the model and observed ages, but the model ages tend to be older than observed. Unfortunately, the cause of this bias in the simulated ages is unknown. The mean age is a diagnostic of integrated transport and, in general, cannot be linked to a single process. There are several possible factors that could be contributing to the bias: The transport out of the boundary layer or within the free troposphere could be too slow in the GMI-MERRA simulation, or it could be because there is too much transport of (old) stratospheric air into the

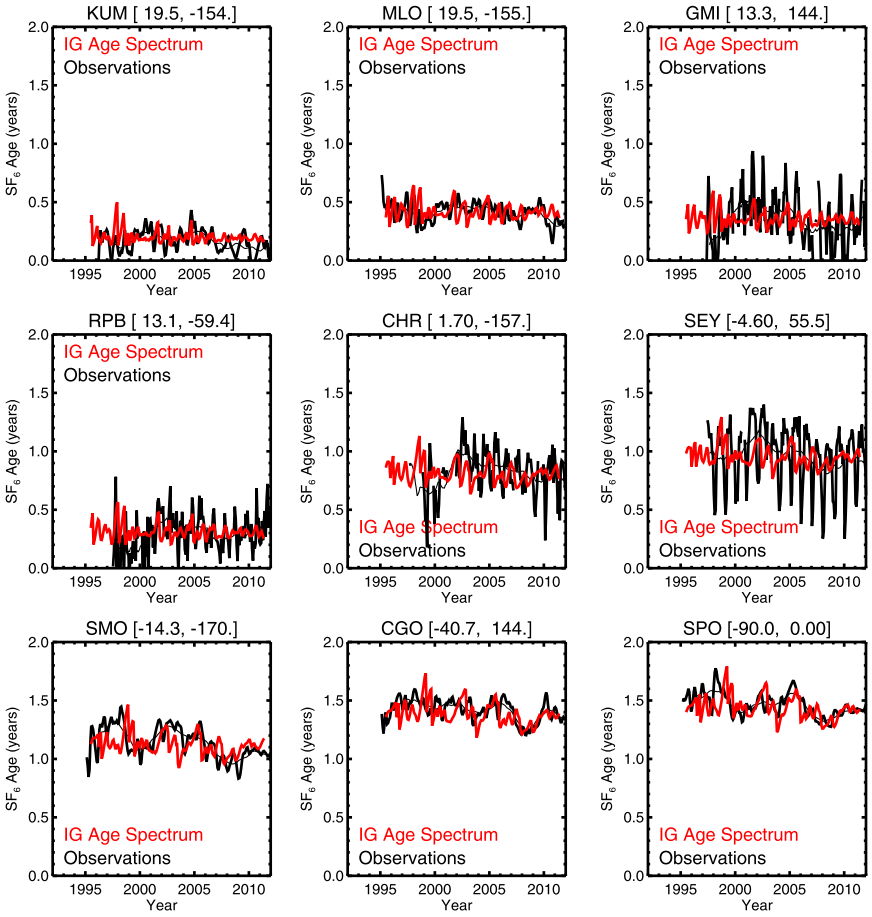

Figure 10. Temporal variations of SF_6 age at several surface locations for observations (black curves) and calculations of SF_6 assuming steady flow with age spectra given by IG distributions with $\Delta = \Gamma$ (red).

troposphere (or a combination of all three). Whether this bias occurs in other models is unknown, and it will be of interest to perform similar comparisons for other simulated meteorology, including that of chemistry-climate models (e.g., within the Stratospheric Processes and Their Role in Climate/International Global Atmospheric Chemistry Chemistry-Climate Model Initiative). This will help evaluate the mean large-scale transport in these models, and may also be useful for studies of variability in tropospheric transport (e.g., seasonal and interannual variations in the transport between hemispheres).

[53] This study has focused solely on SF_6, but there are also measurements of other tracers that could provide additional information on transport time scales. In particular, tracers with rapid, nonlinear growth and/or varying tropospheric lifetimes (e.g., CFC replacement gases or nonmethane hydrocarbons) could provide constraints on the distribution of transit times from the NH midlatitude region. We have also considered only transport from NH midlatitudes, and tracers with different sources may provide constraints of the transport times from other regions.

Appendix A: Impact of Nonlinearities on SF_6 Age

[54] We examine here the potential impact of nonlinearities in the SF_6 growth rate. Although the reference SF_6 time series is approximately linear, the growth rate varies on both seasonal and interannual time scales (see Figure 2). These nonlinearities in the reference time series can cause temporal variations in the SF_6 age even if there are no temporal variations in the transport time [see *Waugh et al.*, 2003].

[55] We generate synthetic time series of SF_6 (and SF_6 age) assuming there is steady flow with an age spectrum $G(t)$ given by an inverse Gaussian (IG) distribution. Specifically, the SF_6 concentration time series is given by

$$C(\tau) = \int_0^\infty C_0(\tau - \tau')G(\tau')\mathrm{d}\tau',$$

where $C_0(t)$ is the reference SF_6 time series,

$$G(t) = \sqrt{\frac{\Gamma^3}{4\pi\Delta^2 t^3}}\ \exp\left(\frac{-\Gamma(t-\Gamma)^2}{4\Delta^2 t}\right),$$

Γ is the mean age, and Δ the width of the spectrum. IG distributions are the age spectra for one-dimensional flow with constant advection and diffusion (or one-dimensional flow with mass-weighted diffusion) and have also shown to be a reasonable approximation of the age spectra in three-dimensional models [*Waugh and Hall*, 2002]. Furthermore, similar synthetic tracer calculations have been performed in the context of stratospheric chlorine [*Waugh et al.*, 2001] and ocean transport and carbon uptake [e.g., *Waugh et al.*, 2004].

[56] The red curves in Figure 10 show the evolution of the SF_6 age from the synthetic SF_6 generated using IG

distributions for the age spectra, where the mean age and width of the spectra are equal to the time-mean SF_6 age from stations. (Equation 1 is used for the age calculations and no assumption regarding linear growth is made.) Although the transport is steady, there are temporal variations in the synthetic SF_6 age. These temporal variations can be traced back to variations in the reference time series (Figure 2). During periods where the tracer growth rate increases (decreases) with time, the tracer age will decrease (increase) even if the transport is steady. The growth rate of SF_6 (in NH middle latitudes) increased between 1998 and 2008, and decreased before and after this period (Figure 2). Consistent with this, there is general decrease in synthetic SF_6 age between the late 1990s and late 2000s in the age spectra calculations for older mean ages.

[57] For locations with SF_6 age less than a year, the amplitude of the temporal variations in the synthetic SF_6 age is much smaller than variations in the observed SF_6 age (black curves in Figure 10), and the observed seasonal and interannual variations in the tropics are unlikely to be caused by nonlinearities in the SF_6 growth. However, for older ages (southern subtropics and higher latitudes), the variations are of similar magnitude to those for the observed SF_6 age at SH middle and high latitudes. Hence, for these stations, the temporal variations in the SF_6 age due to nonlinearities in the reference time series could be contributing to some of the temporal variations in the observed SF_6 age.

[58] **Acknowledgments.** The HIPPO data were downloaded from http://hippo.ornl.gov/ except for the tropopause measurements that were provided by NCAR/EOL (http://data.eol.ucar.edu/), under sponsorship of the National Science Foundation. The HIPPO mission was supported by the National Science Foundation, NOAA, and Harvard University. The HATS ground-based observations are funded partially by the Atmospheric Chemistry, Carbon Cycle, and Climate program (AC4) (formerly Atmospheric Composition and Climate Program) of NOAA's Climate Program Office and NOAA OAR Base Funds. We thank the GMI core modeling team, which receives funding from the NASA MAP program.

References

Adler, R. F., et al. (2003), The Version 2 Global Precipitation Climatology Project (GPCP) monthly precipitation analysis (1979–present), *J. Hydrometeor.*, *4*, 1147–1167.

Denning, A. S., et al. (1999), Three-dimensional transport and concentration of SF_6: A model intercomparison study (TransCom 2), *Tellus*, *51B*, 266–297.

EDGARv4.2 Source: European Commission, Joint Research Centre (JRC)/ Netherlands Environmental Assessment Agency (PBL) (2011), Emission Database for Global Atmospheric Research (EDGAR), release version 4.2, http://edgar.jrc.ec.europa.eu.

Elkins, J. W., T. M. Thompson, T. H. Swanson, J. H. Butler, B. D. Hall, S. O. Cummings, D. A. Fisher, and A. G. Raffo (1993), Decrease in the growth rates of atmospheric chlorofluorocarbons 11 and 12, *Nature*, *364*, 780–783.

Elkins, J. W., F. L. Moore, and E. S. Kline (2002), Update: New airborne gas chromatograph for NASA airborne platforms, *Proceedings of the Earth Science Technology Conference*, 1–3.

Engel, A., et al. (2006), Highly resolved observations of trace gases in the lowermost stratosphere and upper troposphere from the Spurt project: An overview, *Atmos. Chem. Phys.*, *6*, 283–301.

England, M. H. (1995), The age of water and ventilation timescales in a global ocean model, *J. Phys. Oceanogr.*, *25*, 2,756–2,777.

Fahey, D. W., et al. (2006), Altair unmanned aircraft system achieves demonstration goals, *EOS Trans. Am. Geophys. Union*, *87*(20), 197–201, doi:10.1029/2006EO200002.

Geller, L. S., J. W. Elkins, J. M. Lobert, A. D. Clarke, D. F. Hurst, J. H. Butler, and R. C. Myers (1997), Tropospheric SF_6: Observed latitudinal distribution and trends, derived emissions and interhemispheric exchange time, *Geophys. Res. Lett.*, *24*, 675–678.

Gloor, M., E. Dlugokencky, C. Brenninkmeijer, L. Horowitz, D. F. Hurst, G. Dutton, C. Crevoisier, T. Machida, and P. Tans (2007), Three-dimensional SF_6 data and tropospheric transport simulations: Signals, modeling accuracy, and implications for inverse modeling, *J. Geophys. Res.*, *112*, D15112, doi:10.1029/2006JD007973.

Hall, B. D., G. S. Dutton, D. J. Mondeel, J. D. Nance, M. Rigby, J. H. Butler, F. L. Moore, D. F. Hurst, and J. W. Elkins (2011), Improving measurements of SF_6 data for the study of atmospheric transport and emissions, *Atmos. Meas. Tech.*, *4*(11), 2441–2451.

Harnisch, J., R. Borchers, P. Fabian, and M. Maiss (1996), Tropospheric trends for CF_4 and C_2F_6 since 1982 derived from SF_6 dated stratospheric air, *Geophys. Res. Lett.*, *23*, 1099–1102.

Holzer, M., and G. J. Boer (2001), Simulated changes in atmospheric transport climate, *J. Climate*, *14*, 4398–4420.

Levin, I., and V. Hesshaimer (1996), Refining of atmospheric transport model entries by the globally observed passive tracer distributions of 85krypton and sulfur hexafluoride (SF_6), *J. Geophys. Res.*, *101*, 16,745–16,756.

Levin, I., et al. (2010), The global SF_6 source inferred from long-term high precision atmospheric measurements and its comparison with emission inventories, *Atmos. Chem. Phys.*, *10*, 2,655–2,662, doi:10.5194/acp-10-2655-2010.

Lintner, B. R., A. B. Gilliland, and I. Y. Fung (2004), Mechanisms of convection-induced modulation of passive tracer interhemispheric transport interannual variability, *J. Geophys. Res.*, *109*, D13102, doi:10.1029/2003JD004306.

Moore, F. L., et al. (2003), Balloonborne in situ gas chromatograph for measurements in the troposphere and stratosphere, *J. Geophys. Res.*, *108*(D5), 8330, doi:10.1029/2001JD000891.

Morris, R. A., T. M. Miller, A. A. Viggiano, J. F. Paulson, S. Solomon, and G. Reid (1995), Effects of electron and ion reactions on atmospheric lifetimes of fully fluorinated compounds, *J. Geophys. Res.*, *100*, 1287–1294.

Neu, J. L., and R. A. Plumb (1999), The age of air in "leaky pipe" model of stratospheric transport, *J. Geophys. Res.*, *104*, 19,243–19,255.

Patra, P. K., S. Lal, and B. H. Subbaray (1997), Observed vertical profile of sulfur hexafluoride (SF_6) and its atmospheric applications, *J. Geophys. Res.*, *102*, 8855–8859.

Patra, P. K., M. Takigawa, G. S. Dutton, K. Uhse, K. Ishijima, B. R. Lintner, K. Miyazaki, and J. W. Elkins (2009), Transport mechanisms for synoptic, seasonal and interannual SF_6 variations and "age" of air in troposphere, *Atmos. Chem. Phys.*, *9*, 1209–1225.

Peters, W., M. C. Krol, E. J. Dlugokencky, F. J. Dentener, P. Bergamaschi, G. Dutton, P. v. Velthoven, J. B. Miller, L. Bruhwiler, and P. P. Tans (2004), Toward regional-scale modeling using the two-way nested global model TM5: Characterization of transport using SF_6, *J. Geophys. Res.*, *109*, D19314, doi:10.1029/2004JD005020.

Prinn, R., D. Cunnold, P. Simmonds, F. Alyea, R. Boldi, A. Crawford, P. Fraser, D. Gutzler, D. Hartley, and R. Rosen (1992), Global average concentration and trend for hydroxyl radicals deduced from ALE/GAGE trichloroethane (methyl chloroform) data for 1978–1990, *J. Geophys. Res.*, *97*, 2445–2461.

Ravishankara, A. R., S. Solomon, A. A. Turnipseed, and R. F. Warren (1993), The atmospheric lifetimes of long-lived halogenated species, *Science*, *259*, 194–199.

Ray, E. A., F. L. Moore, J. W. Elkins, G. S. Dutton, D. W. Fahey, H. Vömel, S. J. Oltmans, and K. H. Rosenlof (1999), Transport into the Northern Hemisphere lowermost stratosphere revealed by in situ tracer measurements, *J. Geophys. Res.*, *104*, 26,565–26,580.

Rienecker, M. M., et al. (2011), MERRA: NASA's Modern-Era Retrospective Analysis for Research and Applications, *J. Climate*, *24*, 3624–3648.

Strahan, S. E., B. N. Duncan, and P. Hoor (2007), Observationally derived transport diagnostics for the lowermost stratosphere and their application to the GMI chemistry and transport model, *Atmos. Chem. Phys.*, *7*, 2435–2445.

Waugh, D. W., and T. M. Hall (2002), Age of stratospheric air: Theory, observations, and models, *Rev. Geophys.*, *40*(4), 1,010, doi:10.1029/2000RG000101.

Waugh, D. W., D. B. Considine, and E. L. Fleming (2001), Is upper stratospheric chlorine decreasing as expected?, *Geophys. Res. Lett.*, *1187–1190*.

Waugh, D. W., T. M. Hall, and T. W. N. Haine (2003), Relationships among tracer ages, *J. Geophys. Res.*, *108*(5), 3138, doi:10.1029/2002JC001325.

Waugh, D. W., T. W. N. Haine, and T. M. Hall (2004), Transport times and anthropogenic carbon in the subpolar North Atlantic Ocean, *Deep-Sea Res.*, *51*, 1475–1491.

Wofsy, S. C. (2011), HIAPER Pole-to-Pole Observations (HIPPO): Fine-grained, global-scale measurements of climatically important atmospheric gases and aerosols, *Phil. Trans. Roy. Soc. A*, *369*, 2,073–2,086, doi:10.1098/rsta.2010.0313.

Wofsy, S. C., et al. (2012), HIPPO Merged 10-second Meteorology, Atmospheric Chemistry, Aerosol Data (R_20121129), Carbon Dioxide Information Analysis Center, Oak Ridge National Laboratory, Oak Ridge, Tennessee, U.S.A., doi:10.3334/CDIAC/hippo_010.